Metal Processing Technology
Coursework 3

Department of Mechanical Engineering

Imperial College London

Yuxuan Liu

Mohamed Saeed

Xinyang Yuan

Hongze Zou

April 27, 2018

Abstract

Artificial ageing is a critical post-forming process, which can significantly improve material properties (e.g. strength, and toughness). Artificial ageing has been widely adopted in the industry, and recent studies have focused on the development of multi-stage ageing that can potentially increase both a material's post-forming strength and shorten the total artificial ageing time. Over the past decade, there have been many attempts in modeling the material behavior during ageing, however, these models fail to capture the dislocation's effect. Consequently, the following study focuses on the development of an ageing functional module that can model the pre-strained material post ageing strength.

Our implemented ageing module captures material micro-structural state by modeling the time evolution of four physical variables during the ageing process: (1) normalized dislocation density, $\overline{\rho}$, (2) solute concentration, C, (3) precipitate volume fraction, f, and (4) mean precipitate radius. Various numerical integration methods, e.g., Euler method, Range-Kutta 4, Gaussian quadrature, were used to ensure accurate prediction. The entire program is designed vectorially from the beginning, and the code also utilizes the *MATLAB* multi-thread toolbox, therefore system running time can be significantly shortened by benefiting from a single program multiple data (SPMD).

By building the functional module, we can quickly estimate the optimum ageing conditions, such as ageing temperature and time, which significantly fasten the component's design process. Therefore, it is essential to simulate the ageing process to optimise and improve the application of these high strength aluminium alloys. The aim of this project is to predict the post-form strength of the AA6082 aluminium alloy and simulate the multi-stage ageing process.

It was found that the two-stage ageing process saves overall ageing time compared to the one-stage ageing process, but usually at the cost of a slightly lower post-form strength. The optimum condition was found to be when the first-stage ageing temperature is high and the first-stage ageing time greater than 7 minutes.

Contents

1 Aim and background **1**

2 Numerical Model **3**

2.1 Notation 3

2.2 Numerical Integration 3

2.3 Viscoplastic Model 5

2.4 Ageing Model 6

2.5 Multistage Ageing Model 8

3 Full Assembly **10**

3.1 Flowchart of Overall Ageing Module 10

3.2 Notation Convention 10

3.3 Single Program,Multiple Data (SPMD) Optimization 16

3.4 Numerical Fitting 17

4 Modelling Validation **17**

4.1 Viscoplastic Model Validation 17

4.2 One-Stage Ageing Model Validation 18

5 Implementation of the functional modules **19**

5.1 Criteria 20

5.2 One-Stage Artificial Ageing 21

5.3 Two-Stage Artificial Ageing 21

5.4 Application of ageing module on PAMSTAMP 23

5.5 Implementation of Interfacial Heat Transfer Coefficient Model 23

6 Conclusion **24**

7 References **25**

1 Aim and background

The aim of this report is to develop a post-form strength prediction module that can be embedded in a Finite Element (FE) software to predict strength evolution of formed components after multiple stage artificial ageing.

Precipitation hardening or ageing is the process in which materials harden over a prolonged time. Ageing is a heat treatment technique that increases the strength of aluminium alloys (and most other structural alloys) by the materialization of second phase particles (impurities) within the original phase matrix [1]. Second phase particles distort the lattice by preventing the movement of dislocations (dislocation pinning) and thus the dislocations have to go around the particles or cut through them, as a result, the aluminium is stronger [1].

Ageing is a complicated process which involves many individual strengthening effects, the process is simplified to the three stages below:

- **Solution heat treatment**, the first stage, is the process of heating up the aluminium to temperature 450°C - 520°C (temperature between solvus and solidus states) in which the second phase particles dissolve deeply into the matrix.
- **Quenching** is the second stage, the solid solution is rapidly cooled at room temperature. The quenching stage only takes a few seconds and as such not all the alloying elements can precipitate, this reduces solubility and as a result a supersaturated solid solution (SSSS) forms.
- **Precipitation hardening** the final stage, artificial ageing is achieved by increasing the temperature again to approximately 120°C (below solvus temperature). Elevating the temperature forces the alloying element out of the matrix, the decomposition of the SSSS and as a consequence, strengthening precipitates are formed. The strength of these precipitates is governed by their intermolecular distance. The precipitation sequence for structured alloys is shown in the figure 1 below.

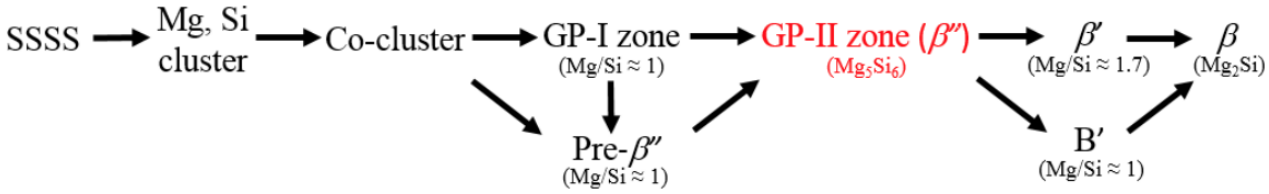

Figure 1: Precipitation sequence of common structural alloys [2]

Modeling of the post-form strength of aluminium and other structural alloys is becoming increasingly important as they are being used extensively in the automotive and aerospace industries. Modeling the micro structure evolution can help improve the manufacturing and application of high strength alloys [1,3]. Existing modeling techniques present frameworks based on the precipitation process which is subdivided into three mechanisms; nucleation, growth and coarsening. The list below outlines the two conventional methods of modeling precipitation kinetics:

1. **Kampann and Wagner Numerical model** (KWN) is the approach which attempts to describe the particle size distribution and the nucleation-growth-coarsening phenomena

assuming that the particle is continuous [1,5,6]. A strength model then calculates the changes in hardness by considering the lattice resistance, solid solution hardening and precipitation hardening.

2. **Shercliff-Ashby process model** assumes only one average particle size and the physical elementary mechanisms: nucleation, growth and coarsening are processed individually. It is assumed that a process can only begin given that the previous process was completed [1,7].

The limitations of the approaches mentioned above is the inability to model the pre-strain and thus the approaches cannot predict the post-form strength of workpieces stamped by Fast light Alloys Stamping (FAST). FAST is currently used to manufacture complex aluminium geometries and workpieces [2]. The technique effectively heats the workpiece rapidly (approximately 50°C/s); the workpiece is then transfered to the press. The workpiece is instantaneously pressed and as the heat loss is minimal, formability is adequate. Finally the workpiece is quenched in a cold die to the critical quenching rate. As seen in the figure 2 below, FAST process avoids the solution heat treatment, reduces artificial ageing, consequently the process outputs a superior production rate.

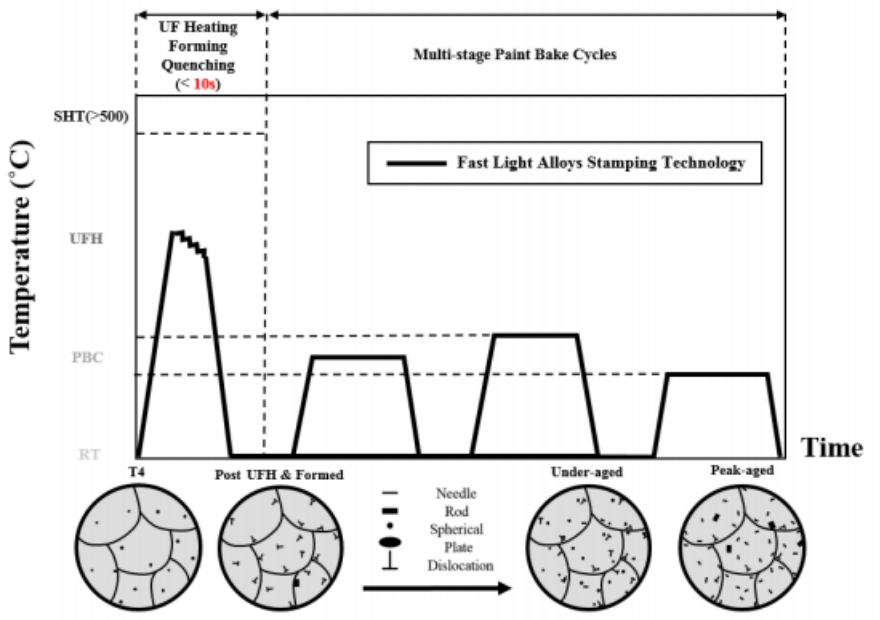

Figure 2: FAST process [2]

As aforementioned the previous modeling approaches are not suitable to model the FAST manufacturing process because of the great influence of the previously existing precipitates and dislocations. Therefore, this paper presents a post-form strength prediction model that characterizes FAST. The model simulates: a) the stress-strain behavior and micro-structural evolution in stamping stage by developing viscoplastic constitutive equations; b) the evolution of material yield strength during artificial ageing via modeling the variations in micro-structural variables, i.e., normalized dislocation, alloy solute concentration and precipitate volume fraction, and mean precipitate radius; c) multi-stage artificial ageing process via modifying the single stage model with material variable time shifts.

2 Numerical Model

2.1 Notation

For the consistency of the presentation, the material variable is presented in the following notation (normalized dislocation is used as an example):

$$\overline{\rho}^{(m)}_{\langle T \rangle} \tag{1}$$

The value in superscript parenthesis notates the ***element number***, and it has range of **[1,m]**. The value in the subscript angle bracket notates the ***time step***, and it has range of **[0,T]**. (note: m is the total number of elements in a model; T is the total time during ageing/viscoplastic stage.n is also used in the following text, which represents the total number of stages.).

2.2 Numerical Integration

2.2.1 Euler Forward Method

The Euler forward method is the simplest numerical integration technique, which uses first order derivative to estimate the function value at the next time step

$$\overline{\rho}_{\langle t+1 \rangle} = \overline{\rho}_{\langle t \rangle} + \Delta t \cdot \dot{\overline{\rho}}_{\langle t \rangle} \tag{2}$$

where Δt is the step size. The geometric interpretation is illustrated in figure 3. Euler forward method is a first order numerical integration technique, i.e., (1) the numerical integration can provide exact solution of first order polynomial; (2) the global error is proportional to the time step. Consequently, a small time step is needed to minimize the integration error.

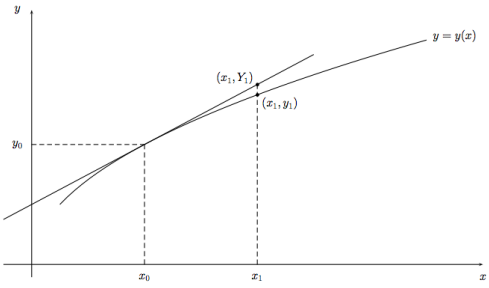

Figure 3: Euler Forward Method [10]

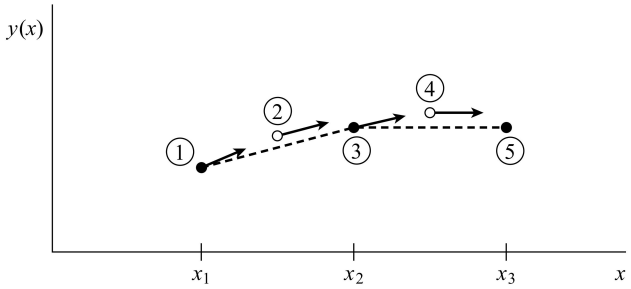

Figure 4: Runge-Kutta Method [11]

2.2.2 Runge-Kutta 4th Order (RK4)

Runge-Kutta (RK) is in the general family of numerical integration (note: Euler method is the first order Runge-Kutta method). Unlike Euler method, the RK method evaluates function gradient at multiple points between time t and time $t + 1$ instead of one, then performs the update (figure 4). (Note: RK can be derived from Taylor expansion, however, the geometric

interpretation is more intuitive for understanding). RK numerical integration has the general form:

$$\overline{\rho}_{\langle t+1\rangle} = \overline{\rho}_{\langle t\rangle} + \Delta t \cdot \sum_{i}^{s} w_i k_i \tag{3}$$

where the k_i is the approximated increment at various point between t and $t+1$, and w_i is the weights of approximated increments. For our numerical model, we used 4th order RK method (or 4-stage RK), because a 4-step update is a good balance of computational cost between each update and accuracy:

$$\overline{\rho}_{\langle t+1\rangle} = \overline{\rho}_{\langle t\rangle} + \Delta t \cdot \left(\frac{1}{6}k_1 + \frac{1}{3}k_2 + \frac{1}{3}k_3 + \frac{1}{6}k_4\right) \tag{4}$$

where,

$$\begin{aligned}
k_1 &= \dot{\overline{\rho}}\left(t, \overline{\rho}_{\langle t\rangle}\right) \\
k_2 &= \dot{\overline{\rho}}\left(t + \Delta t/2, \overline{\rho}_{\langle t\rangle} + \Delta t \cdot k_1/2\right) \\
k_3 &= \dot{\overline{\rho}}\left(t + \Delta t/2, \overline{\rho}_{\langle t\rangle} + \Delta t \cdot k_2/2\right) \\
k_4 &= \dot{\overline{\rho}}\left(t + \Delta t, \overline{\rho}_{\langle t\rangle} + \Delta t \cdot k_3\right)
\end{aligned}$$

RK-4 is 4th order method, therefore, (1) it can calculate exact solution for polynomial equal or below 4th order, and (2) the global numerical error is proportional to the 4th order of time-step.

2.2.3 Trapezoidal Rule

Trapezoidal rule is used to approximate the definite integral, which the integral value is estimated by the trapezium enclosed by the lower and upper bound of the function figure 5:

$$\int_{t}^{t+\Delta t} \overline{\rho}(t)dt \approx \frac{\Delta t}{2} \cdot \left(\overline{\rho}_{\langle t+1\rangle} + \overline{\rho}_{\langle t\rangle}\right) \tag{5}$$

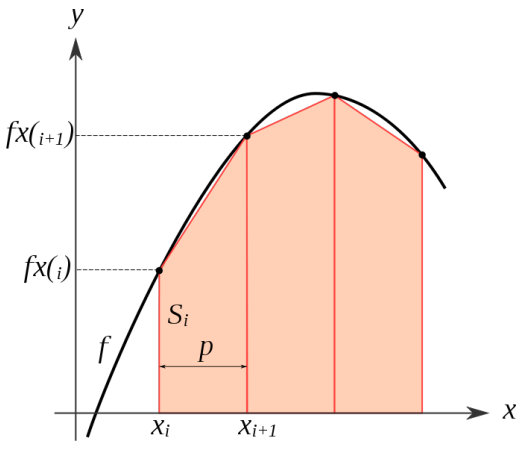

Figure 5: Trapezoidal Method [8]

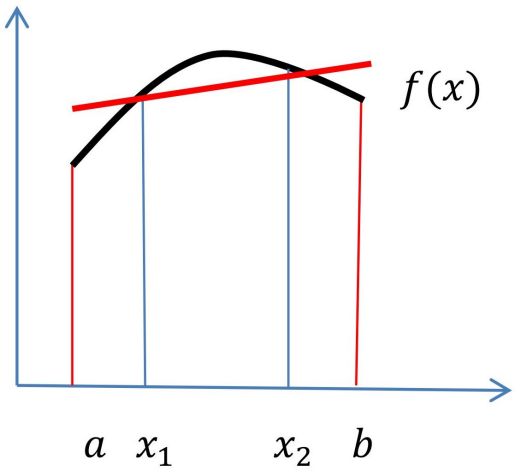

Figure 6: Gaussian Quadrature Method [9]

2.2.4 Gaussian Quadrature

Gaussian quadrature is numerical method of calculating definite integral. The definite integral is approximated via evaluating function values at a set of suitable points and weights:

$$\int_{-1}^{1} \overline{\rho}(t)dt \approx \sum_{i}^{n} w_i \overline{\rho}(t = x_i) \tag{6}$$

By shifting the integration boundary, we can obtain an approximate definite integral over arbitrary range:

$$\int_{b}^{a} \overline{\rho}(t)dt \approx \frac{b-a}{2} \sum_{i}^{n} w_i \cdot \overline{\rho} \left(\frac{b-a}{2} x_i + \frac{a+b}{2} \right) \tag{7}$$

In our model implementation, we use 4-point Gaussian quadrature, which can yield exact result for polynomials equal to or less than 7th (i.e. $2n-1$) order.The values evaluation points, x_i, and weight values, w_i, are listed in table 1.

Table 1: Weight for each Gaussian node

x_1	x_2	x_3	x_4
-0.86	-0.33	0.33	0.86
w_1	w_2	w_3	w_4
$\frac{18-\sqrt{30}}{36}$	$\frac{18+\sqrt{30}}{36}$	$\frac{18+\sqrt{30}}{36}$	$\frac{18-\sqrt{30}}{36}$

2.2.5 Notation on Numerical Method

For the simplicity of following the report, abbreviated functional notation is used refering numerical methods presented in this section:

E{} $\longrightarrow$ Euler Forward Method
RK{} $\longrightarrow$ Runge-Kutta 4
T{} $\longrightarrow$ Trapezoidal Rule
GQ{} $\longrightarrow$ Gaussian Quadrature

2.3 Viscoplastic Model

Viscoplastic model describes the stress-strength relationship during the rate dependent plastic deformation process. For the implementation of our ageing functional module, viscoplastic model is used to predict the normalized dislocation, $\overline{\rho}$, introduced to the component during the stamping process.

2.3.1 Constitutive Relationship

The constitutive equations of viscoplastic model is presented below, where ϵ_p is the plastic deformation; R or σ_{dis} is the dislocation hardening; and $\overline{\rho}$ is the normalized dislocation.

$$\dot{\epsilon_p} = \Big(\frac{\overline{\sigma} - R - k}{K}\Big)^{n_1} \tag{8}$$

$$\dot{R} = 0.5B\overline{\rho}^{-0.5}\dot{\overline{\rho}} \tag{9}$$

$$\dot{\overline{\rho}} = A(1-\overline{\rho})\dot{\epsilon_p} - C\overline{\rho}^{n_2} \tag{10}$$

$$\overline{\sigma} = E(\epsilon_T - \epsilon_p) \tag{11}$$

2.4 Ageing Model

2.4.1 Equation of States

During the post-forming artificial ageing process,the material yield strength depends on four material micro-structural variables (i.e. variables define the material micro-structural states): (1) normalized dislocation, $\overline{\rho}$; (2) alloy solute concentration, C_t; (3) volume fraction of precipitate, f_t;(4) radius of precipitates, r:

$$\sigma_y \rightarrow f(\overline{\rho}, C_t, f_t, r) \tag{12}$$

2.4.2 Normalized Dislocation

Dislocations were generated in the component during the forming stage, which not only strengthens the material via strain hardening mechanism, but also affect material ageing growth in post forming. The time evolution of material normalized dislocation follow exponential law and the rate is governed by the coefficient, C_{ageing}:

$$\dot{\overline{\rho}} = -C_{ageing} \cdot \overline{\rho}^{n_2} \tag{13}$$

2.4.3 Alloy Solute Concentration

The solute concentration, C, is the concentration of alloy elements that are dissolved in the aluminium matrix (i.e. the solvent). Equilibrium concentration, C_e, value is determined by the temperature via Arrhenius law equation (15). Non-equilibrium state can be achieved during the quenching process, which the solute concentration is much higher than the equilibrium value, because there isn't enough time for alloy elements to diffuse out of aluminium matrix during quenching.

$$C_e = A_o \cdot e^{\frac{Q_s}{RT}} \tag{14}$$

where Q_s is the solvus boundary enthalpy. Alternatively, the equilibrium concentration at various temperatures can be represented as a fraction of maximum possible concentration,C_s, which occurs at T_s (i.e. metastable solid solvus temperature):

$$C_e = C_s \cdot e^{\frac{Q_s}{R}\left(\frac{1}{T} - \frac{1}{T_s}\right)} \tag{15}$$

The solute alloys will diffuse out of aluminium matrix and form alloy precipitates during ageing process, and the time evolution of the solute concentration during te ageing process follow exponential law [2]:

$$C = C_e + (C_i - C_e) \cdot e^{\frac{t}{\tau}} \tag{16}$$

where C_i is the initial solute concentration before the ageing process, and τ is the time decay constant ($\tau = k \cdot t_p$). Stamping process introduced dislocations to the formed component, which will change the evolution of solute concentration during ageing. In order to capture the effect of dislocation (pre-straining), a second term is added to the exponential law:

$$\dot{C} = A_1 \left(\frac{C_e - C_i}{\tau} \cdot e^{-\frac{-t}{\tau}} \right) + B_1 \cdot \overline{\rho} \tag{17}$$

2.4.4 Yield Strength

The material yield strength is the sum of five individual hardening components (note: σ_{ppt} is not counted, since it can be represented by other two hardening mechanisms):

$$\sigma_y = \sigma_{ds} + \sigma_{ss} + \sigma_i + \frac{\sigma_{by} \cdot \sigma_{sh}}{\sigma_{by} + \sigma_{sh}} \tag{18}$$

where,

$$\sigma_{sh} = C_2 \cdot f^{\frac{1}{2}} \cdot r^{\frac{1}{2}} \tag{19}$$

$$\sigma_{by} = C_3 \cdot f^{\frac{1}{2}} \cdot r^{-1} \tag{20}$$

$$\sigma_{ss} = C_4 \cdot C^{\frac{2}{3}} \tag{21}$$

$$\sigma_{dis} = A_d \cdot \overline{\rho}^{0.5} \tag{22}$$

2.4.5 Volume Fraction of Precipitate

Similar to the solute concentration, volume fraction of precipitate also indicates the amount of alloy elements in the aluminium matrix. In order to simplify the model, all precipitates have identical chemical composition and thermodynamic properties (note: the chemical composition of precipitates actually vary, as they are made up by different percentages of aluminium and other alloy elements). With the simplification, the volume fraction is negatively and directly proportional to the solute concentration:

$$f = \left(\frac{C_i - C}{C_i - C_e} \right) \cdot f_e \tag{23}$$

The maximum volume fraction, f_max, is achieved at a certain temperature, such that all alloy elements escape from the aluminium matrix, and we can obtain the following condition under such extreme conditions:

$$f_{max} = \left(\frac{C_s - 0}{C_s - C_e} \right) \cdot f_e \tag{24}$$

Consequently, the time evolution of volume fraction, f, can be derived using equations (15), (16), (23), and (24):

$$\begin{aligned} f &= \left(\frac{C_i - C}{C_i - C_e} \right) \cdot f_e \qquad (25) \\ &= f_{max} \cdot \left(\frac{C_s - C_e}{C_s} \right) \left(\frac{C_i - C}{C_i - C_e} \right) \\ &= f_{max} \cdot \left(1 - \frac{C_e}{C_s} \right) \cdot \frac{1}{(C_i - C_e)} \left(C_i - C_e - (C_i - C_e) \cdot e^{\frac{t}{\tau}} \right) \\ &= f_{max} \cdot \left(1 - e^{\frac{Q_s}{R}\left(\frac{1}{T} - \frac{1}{T_s}\right)} \right) \cdot \left(1 - e^{-\frac{t}{\tau}} \right) \qquad (26) \end{aligned}$$

Similar to the solute concentration, the time evolution of volume fraction also depends on the material dislocation and can be written as follows:

$$\dot{f} = -\frac{f_e}{C_i - C_e} \cdot \dot{C} \tag{27}$$

$$= -\frac{f_e}{C_i - C_e} \cdot \left(\left(\frac{C_e - C_i}{\tau} \cdot e^{-\frac{-t}{\tau}} \right) + B_1 \cdot \overline{\rho} \right) \tag{28}$$

2.4.6 Mean Radius of Precipitate

Finally, the average radius of precipitates is also a microstructural variable that affects the material post ageing strength, due to the size of precipitates affecting the effectiveness of the dislocation pinning . The growing of the precipitate is determined by the classical cubic coarsening law, where C_1 is the coarsening coefficient, and Q_A is the activation barrier for volume diffusion of atoms among particles [2]:

$$r^3 - r_0^3 = C_1 \cdot \frac{t}{T} e^{\frac{Q_A}{RT}} \tag{29}$$

Similar to the solute concentration of volume fraction, the growth rate of the precipitate also depends on the dislocations:

$$\dot{r} = A_2 \cdot \frac{1}{3} \left(\frac{C_1 \cdot e^{-\frac{Q_A}{RT}}}{T} \right)^{\frac{1}{3}} \cdot t^{-\frac{2}{3}} + B_2 \cdot \overline{\rho} \tag{30}$$

2.5 Multistage Ageing Model

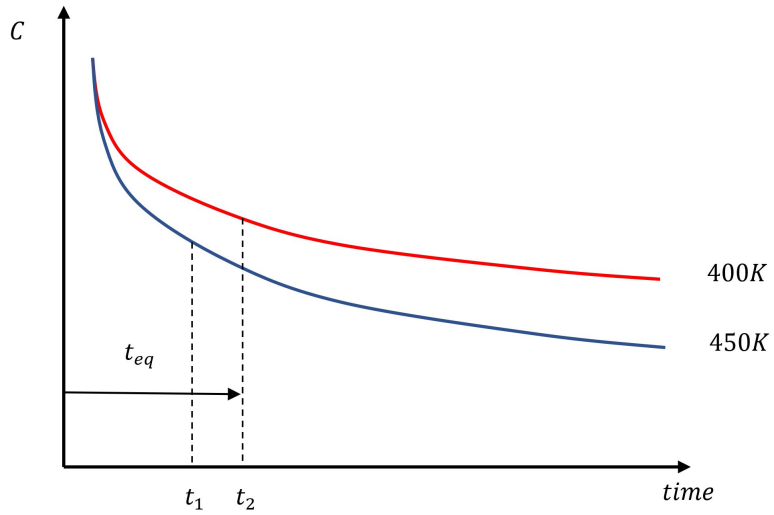

Figure 7: Multisatge of Ageing

The formed component undergoes multiple ageing stages at different temperatures with different ageing times. Having multiple-stage ageing can not only increase the final material post-ageing strength, but also reduce the total ageing time. The following method implements multi-stage ageing via converting the effects of predecessor stages as a time-shift, t_{eq}, in the final stage figure 7. A two-stage example is presented below, and the methodology can be adapted for any number of stages (note: for two-stage, there will only be one time-shift term, t_{eq} for each physical variable. For n-stage ageing, the net time-shift in the final stage will simply be the superposition of time-shifts introduced by each predecessor stage,$t_{eq} = \sum_i^{n-1} t_{eq,i}$).

2.5.1 Time-shift in Solute Concentration

The material solute concentration reaches C_{t1} at the end of stage one. Under stage 2 temperature conditions, the time needed to reach the same solute concentration (i.e. C_{t1}) is t_2.

$$C_{t1} = C_{e1} + (C_i - C_{e1}) \cdot e^{-\frac{t_1}{\tau_1}} \tag{31}$$

$$C_{t1} \rightarrow C_{t2} = C_{e1} + (C_i - C_{e2}) \cdot e^{-\frac{t_2}{\tau_2}} \tag{32}$$

Consequently we can find the timeshift via finding the expression of t_2 in terms of t_1 (note: during simulation the value of t_1 will be the total time of stage-1):

$$t_{eq,C} = t_2 = -\tau_2 \cdot ln\left(\frac{C_{e1} - C_{e2}}{C_i - C_{e2}} + \frac{C_i - C_{e1}}{C_i - C_{e2}} \cdot e^{-\frac{t_1}{\tau_1}}\right) \tag{33}$$

2.5.2 Time-shift in Volume Fraction

Under constant precipitate chemical composition and thermodynamic property assumption, the volume fraction is negatively and directly proportional to the solute concentration. Consequently, the value of time shift in volume fraction is the same as solute concentration's:

$$t_{eq,f} = t_{eq,C} \tag{34}$$

2.5.3 Time-shift in Mean Precipitate Radius

Similar to the method for calculating the timeshift of a solute concentration; the material's mean precipitate radius after first stage ageing is r_1, and the material needs a time of t_2 to achieve the same value of mean precipitate radius:

$$r_{t1} = \frac{t_1}{T_1} \cdot e^{-\frac{Q_A}{RT_1}} \tag{35}$$

$$r_{t1} \rightarrow r_{t2} = \frac{t_2}{T_2} \cdot e^{-\frac{Q_A}{RT_2}} \tag{36}$$

So we can calculate the time shift introduced by stage-1 ageing via:

$$t_{eq,r} = t_2 = \frac{T_2}{T_1} \cdot e^{\frac{Q_A}{RT_2} - \frac{Q_A}{RT_1}} \tag{37}$$

3 Full Assembly

3.1 Flowchart of Overall Ageing Module

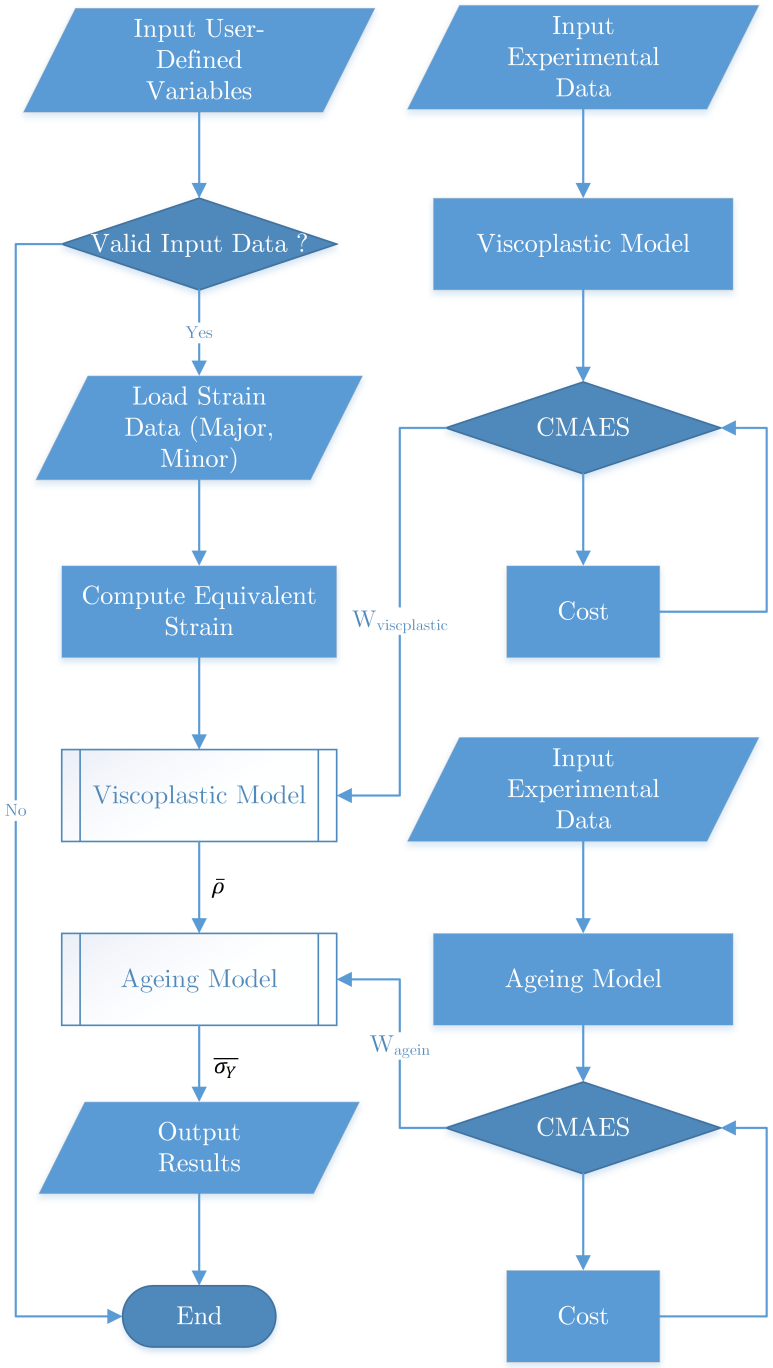

Figure 8: Flowchart of the Overall Ageing Module

3.2 Notation Convention

For the readability of code and consistency of presentation, the array axis definition presented here is used throughout the paper and the final implemented module code.

- **Horizontal axis (rows in 2D array):** this is the elemental axis. To illustrate, the physical variable evolution history (e.g. $\overline{\rho}$) of the 30th element will correspond to the 30th column in the array (which is also a column vector). In text, the 30th element will be referred to as $\overline{\rho}^{(30)}$
- **Vertical axis (columns in 2D array):** this is the time axis. To illustrate, the physical variable values (e.g. $\overline{\rho}$) of all elements at time 30 will correspond to the 30th row in the array (which is also a row vector). In text, the values of all elements at time 30 will referred to as $\overline{\rho}_{\langle 30 \rangle}$

$$\begin{bmatrix} \vdots & \vdots & & \vdots & & \vdots \\ \vdots & \vdots & & \vdots & & \vdots \\ \bar{\rho}^{(1)} & \bar{\rho}^{(2)} & \dots & \bar{\rho}^{(30)} & \dots & \bar{\rho}^{(m)} \\ \vdots & \vdots & & \vdots & & \vdots \\ \vdots & \vdots & & \vdots & & \vdots \end{bmatrix} \qquad \begin{bmatrix} \dots & \dots & \bar{\rho}_{<1>} & \dots & \dots \\ \dots & \dots & \bar{\rho}_{<2>} & \dots & \dots \\ & & \vdots & & \\ \dots & \dots & \bar{\rho}_{<30>} & \dots & \dots \\ & & \vdots & & \\ \dots & \dots & \bar{\rho}_{<T>} & \dots & \dots \end{bmatrix}$$

Moreover, when referring to **time**, there are two definitions: (1) time defined as a numerical time-step, which is represented with angle brackets, e.g., $\rho_{\langle t \rangle}$; (2) time defined as a stage number of *Pamp-Stamp* simulation, represented with cursive brackets, e.g., $\epsilon_{\{t\}}$.

① Export of Pampstamp Data

Before the execution of the ageing module, there are two data series needed to export from the *Pam-Stamp* simulation results during **stamping stages**: (1) major strain distribution among all elements, (2) minor strain distribution among all elements. The major and minor strain are saved as **.asc** format, which are then imported to the *Matlab* **workspace**. The imported data are stored in two 2D arrays (i.e. $[\epsilon_1]$ and $[\epsilon_2]$), which has shape of **(m,n)**. Then equivalent strain value is calculated from the minor strain via the following equation:

$$\epsilon_{eq} = \frac{1}{1+\nu} \cdot \left(\frac{1}{2} \left[(\epsilon_1 - \epsilon_2)^2 + (\epsilon_2 - \epsilon_3)^2 + (\epsilon_3 - \epsilon_1)^2 \right] \right)^{\frac{1}{2}} \tag{38}$$

where the third principal strain component is calculated using constant volume assumption during plastic deformation:

$$\epsilon_3 = -(\epsilon_1 + \epsilon_2) \tag{39}$$

Since only equivalent strain is used for the following calculations, the eq subscript is dropped $\epsilon_{eq} \rightarrow \epsilon$

3.2.1 Matrix Representation of Data Flow

n is the total number of stage during stamping process.

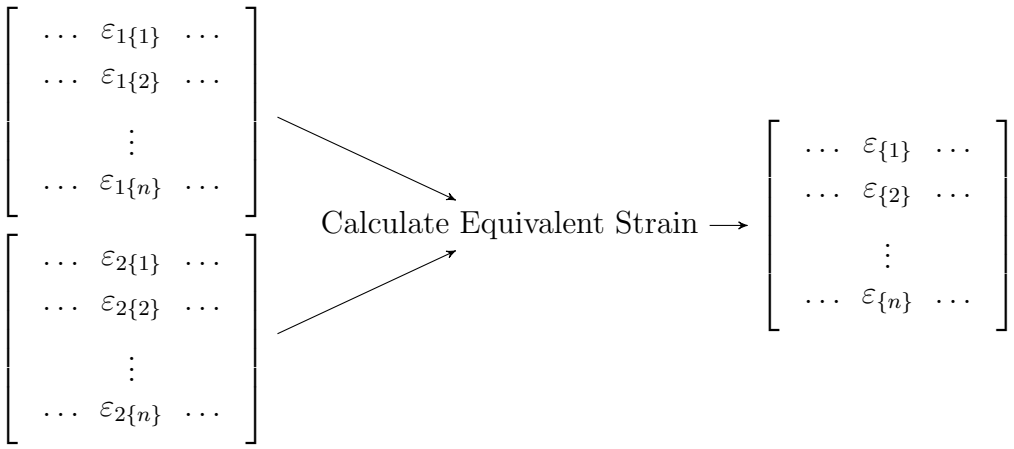

② Strain Interpolation

As shown by figure, there will be an equivalent value at each stage during stamping process. The first stage is taken at time zero, and the second stage time is calculated via:

$$t_{n+1} = t_n + \frac{Prog_{\{n+1\}} - Prog_{\{n\}}}{V_{stamping}} \tag{40}$$

where the $Prog$ is the closing distance of the punch at each stage, and $V_{stamping}$ is the stamping velocity of the punch. Consequently, we can calculate **strain rate** from (1) the time and (2) the equivalent strain at each stage (note: this is also Euler forward method).

$$\dot{\epsilon}_{\{n\}} = \frac{\epsilon_{\{n+1\}} - \epsilon_{\{n\}}}{\Delta t} \tag{41}$$

3.2.2 Variable Timestep

From experiments, the numerical timestep needed for convergence results in the viscoplastic model being negatively correlated to the strain rate, which means a larger strain rate requires a smaller timestep. Therefore, the timestep between two stages will be specifically tuned for strain rate at that stage. The default timestep is chosen to be $\mathbf{0.00001}s$, which is stable for the **strain rate** up to $\mathbf{10}s^{-1}$ (note: the max strain rate for our simulation is only about $2s^{-1}$). Then the timestep will dynamically adjust based on the strain rate criteria shown in the following script (note: the criteria comes from experiments on the viscoplastic model):

```
% calculate step size
    step_size = ones(size(strain_rate)) .* 0.00001;
    step_size(abs(strain_rate) <= 5.0)  = 0.00005;
    step_size(abs(strain_rate) <= 2.0)  = 0.0001;
    step_size(abs(strain_rate) <= 1.0)  = 0.0002;
    step_size(abs(strain_rate) <= 0.5)  = 0.0004;
    step_size(abs(strain_rate) <= 0.5)  = 0.0005;
    step_size(abs(strain_rate) <= 0.1)  = 0.001;
    step_size(abs(strain_rate) <= 0.05) = 0.003;
    step_size(abs(strain_rate) <= 0.01) = 0.008;
    step_size(abs(strain_rate) <= 0.001)= 0.05;
```

3.2.3 Matrix Representation of Data Flow

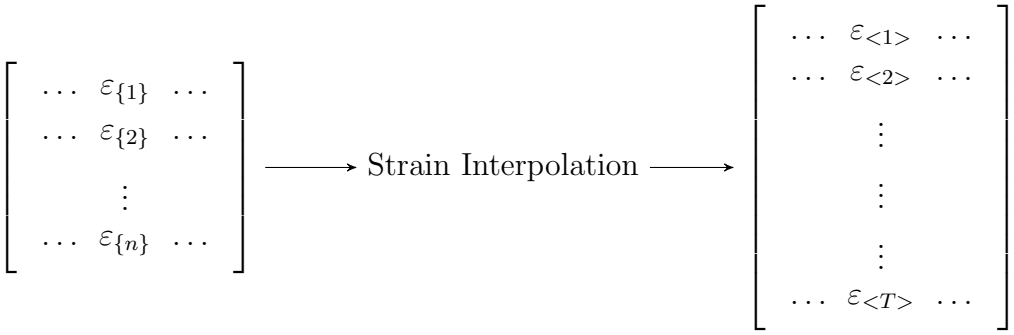

③ Viscoplastic Model

The strain array, $[\epsilon]$, will feed into the viscoplastic model. The constitutive equations for viscoplastic model are presented in section 2.3.1, and will be discretized for the numerical integration. The main loop of the viscoplastic model involves two steps: (1) rate update step, (2) value update step (numeric integration):

Rate update step:

$$\dot{\epsilon}_{p\langle t\rangle} = \left(\frac{E \cdot (\epsilon_{\langle t\rangle} - \epsilon_{p\langle t\rangle}) - R_{\langle t\rangle} - k}{K}\right)^{n1} \tag{42}$$

$$\dot{\rho}_{\langle t\rangle} = A \cdot \left(1 - \overline{\rho}_{\langle t\rangle}\right) \cdot \dot{\epsilon}_{p\langle t\rangle} - C \cdot \overline{\rho}^{n2}_{\langle t\rangle} \tag{43}$$

Value update step:

$$e_{p\langle t+1\rangle} = \mathbf{E}(e_{p\langle t\rangle}, \Delta t) \tag{44}$$

$$\rho_{\langle t+1\rangle} = \mathbf{E}(\rho_{\langle t\rangle}, \Delta t) \tag{45}$$

$$R_{\langle t+1\rangle} = B \cdot (\rho_{\langle t+1\rangle})^{\frac{1}{2}} \tag{46}$$

3.2.4 Value Clipping

The viscoplastic model is very sensitive to the numerical timestep, large numerical timestep will lead to divergence (Fig.9c). From the investigation on th cause of numerical divergence, the cause of divergence is the abnormal value plastic strain rate, $\dot{\epsilon_p}$.

Consequently, a clipping function is introduced to eliminate the divergence issue. The clipping function essentially bounds the value of plastic strain rate, $\dot{\epsilon_p}$, within the range of strain rate, $\dot{\epsilon}$. (note: this is a valid assumption, since the sum of elastic and plastic strain rate is the total strain rate. As $\epsilon \to \infty$, $\dot{\epsilon_p} \to \dot{\epsilon}$. The code implementation of the clipping is shown below:

```
% clipping dep
    dep = ((E.*(strain(i)-ep(i,:))-R(i,:)-k)./K).^(n1);
    dep = (STRAIN_RATE >= 0) * min(dep, STRAIN_RATE) + ...
          (STRAIN_RATE <  0) * max(dep, STRAIN_RATE);
```

The effect of value clipping can be seen in figure 9b, where the simulation is still able to generate stable and relatively accurate result with a time-step that can lead to unstable result under non-clipping model (Fig.9c).

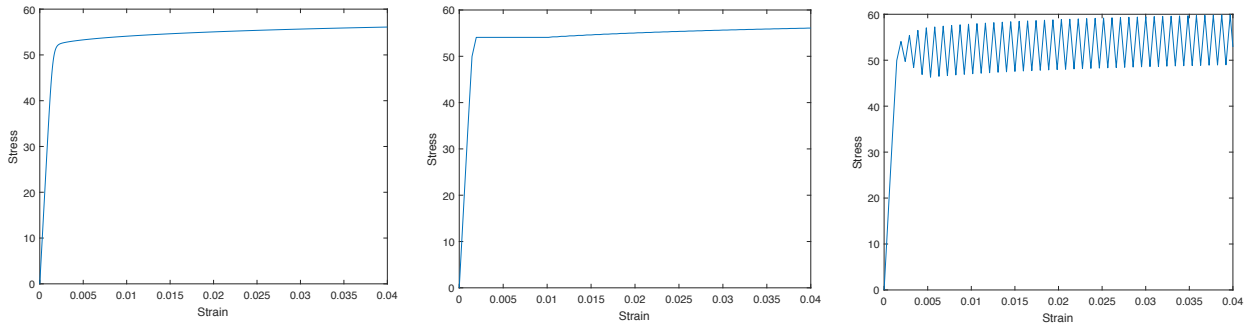

(a) True Result (time-step of 0.0001s) (b) Clipped Result (time-step of 0.0002s (c) Unclipped/Diverged Result (time-step of 0.0002s

Figure 9: Comparision of Simulation Accuracy with Different Numerical Time-step

3.2.5 Matrix Representation of Data Flow

$$\begin{bmatrix} \cdots & \varepsilon_{<1>} & \cdots \\ \cdots & \varepsilon_{<2>} & \cdots \\ & \vdots & \\ & \vdots & \\ & \vdots & \\ \cdots & \varepsilon_{<T>} & \cdots \end{bmatrix} \longrightarrow \text{Viscoplastic Model} \longrightarrow \begin{bmatrix} \cdots & \bar{\rho}_{<T>} & \cdots \end{bmatrix}$$

④Ageing/Multi-stage Ageing

The ageing model will take the normalized dislocation at the final timestep of the viscoplastic model. The details of ageing model is presented in section 2.4. The main loop of ageing model consists of two stages: (1) Runge-Kutta-4 integration of normalized dislocation density, $\overline{\rho}$; (2) Trapezoid integration of the other micro-structural variables, i.e., C, f, and r.

Since the rate of change of normalized dislocation density only depends on itself, we can perform the RK-4 update:

$$\overline{\rho}_{\langle t+1\rangle} = \mathbf{RK}\{\overline{\rho}_{\langle t\rangle}, \Delta t\} \tag{47}$$

Then the rate of other three parameters can be calculated via:

$$\dot{C}_{\langle t\rangle} = A_1 \left(\frac{C_e - C_i}{\tau} \cdot e^{-\frac{-t}{\tau}} \right) + B_1 \cdot \overline{\rho}_{\langle t\rangle} \tag{48}$$

$$\dot{f}_{\langle t\rangle} = -\frac{f_e}{C_i - C_e} \cdot \left(\left(\frac{C_e - C_i}{\tau} \cdot e^{-\frac{-t}{\tau}} \right) + B_1 \cdot \overline{\rho}_{\langle t\rangle} \right) \tag{49}$$

$$\dot{r}_{\langle t\rangle} = A_2 \cdot \frac{1}{3} \left(\frac{C_1 \cdot e^{-\frac{Q_A}{RT}}}{T} \right)^{\frac{1}{3}} \cdot t^{-\frac{2}{3}} + B_2 \cdot \overline{\rho}_{\langle t\rangle} \tag{50}$$

Then, perform trapezoidal integration update on C, f, and r:

$$C_{\langle t\rangle} = \mathbf{T}\{\dot{C_{\langle t\rangle}}\} + C_0 \tag{51}$$

$$f_{\langle t\rangle} = \mathbf{T}\{\dot{f_{\langle t\rangle}}\} + f_0 \tag{52}$$

$$r_{\langle t\rangle} = \mathbf{T}\{\dot{r_{\langle t\rangle}}\} + r_0 \tag{53}$$

where, C_0, f_0,and r_0 are initial conditions of the micro-structural variables. The final step is using the micro-structural states to calculate individual strengthening value and the resultant yield strength.

3.2.6 Correction of Mean Precipitate at First Time-step

At time of zero, the rate of precipitate growth results in math error, therefore, the rate value can only be estimated at the first time-step. Since we implement the RK-4 update on the normalized dislocation, the default time-step chosen is **5s** for the ageing model, which precipitate growth can be significant over the time-step. Consequently, Gaussian quadrature is used to calculate the growth:

$$r_{corr} = \mathbf{GQ}\{\dot{r}_{\langle 0\rangle} \rightarrow \dot{r}_{\langle 1\rangle}\} \tag{54}$$

3.2.7 Multi-Stage Ageing

There are two possible implementations of the multi-stage ageing process: (1) use the ageing model to predict the evolution of micro-structural variables at stage one, then feed the results of the first stage to the ageing model with different time and temperature conditions. However, using such cyclic approach requires to change the ageing model parameters at each stage, since they are temperature dependent. (2) implement the multi-stage ageing model with time-shifts for micro-structural variables, introduced in section 2.4. The main loop is almost identical to the singe ageing model, and the only difference is in the rate calculation step:

$$\dot{C}_{\langle t\rangle} = A_1 \left(\frac{C_e - C_i}{\tau} \cdot e^{-\frac{-t+t_{eq,C}}{\tau}} \right) + B_1 \cdot \overline{\rho}_{\langle t\rangle} \tag{55}$$

$$\dot{f}_{\langle t\rangle} = -\frac{f_e}{C_i - C_e} \cdot \left(\left(\frac{C_e - C_i}{\tau} \cdot e^{-\frac{-t+t_{eq,f}}{\tau}} \right) + B_1 \cdot \overline{\rho}_{\langle t\rangle} \right) \tag{56}$$

$$\dot{r}_{\langle t\rangle} = A_2 \cdot \frac{1}{3} \left(\frac{C_1 \cdot e^{-\frac{Q_A}{RT}}}{T} \right)^{\frac{1}{3}} \cdot (t + t_{eq,r})^{-\frac{2}{3}} + B_2 \cdot \overline{\rho}_{\langle t\rangle} \tag{57}$$

3.2.8 Matrix Representation of Data Flow

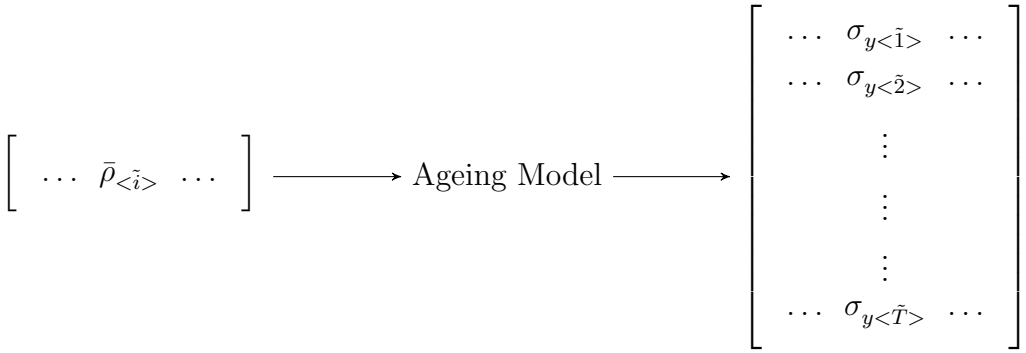

3.3 Single Program,Multiple Data (SPMD) Optimization

The module is designed vectorially from the beginning of the project. All elemental data are stored and computed as row vector. For-loop is eliminated for any elemental-wise calculation, and these calculations are all achieved via array elemental-wise operations (note: the array elemental wise operation is highly optimized by *Matlab*, which computations are efficiently allocated among the cpu threads).

A vectorial implementation example is given below:

```
% rho calculation (RK4)
rho = rungeKutta4(rho_0,C_age,n2,TIMESTEP,TEMPORAL_SIZE);

% C calculation (since dC is calculated from rho, also RK4)
dC = A1 .* ((C_e-C_i)./tau) .* exp(-time./tau) + B1.*rho; % rate
    step
C = cumtrapz(dC,1) .* TIMESTEP + C_0;  % trapezoidal integration
    step

% f calculation (since df is calculated from rho, also RK4)
df = -(f_e./(C_i - C_e)) .* dC;      % rate step
f = cumtrapz(df,1) .* TIMESTEP + f_0; % trapezoidal integration step
```

Moreover, system also utilize the *Matlab* parallel toolbox for large elemental array calculation, such as the array has elemental dimension more than 10,000. The elemental calculation are allocated to different cpu cores, and calculations on multi-elements are taken concurrently. (note: the module takes about 2 minutes to simulate 10-hour ageing for FEA model with 13,000 elements) An example parallel thread implementation is shown below:

```
% main loop
parfor element_idx = 1:NUMBER_ELEMENTS
        initial_condition = [0,0,0,0];
        for time_idx = 1:(NUMBER_STAGES-1) ......
        end
end
```

3.4 Numerical Fitting

The implementation of numerical fitting is detailedly covered in section 3 to section 4 from coursework 1 report [4]. In summary, the covariance matrix adaptive evolution strategy (**CMA-ES**) is implemented for the fitting process. The CMA-ES is extremely suitable for non-concave, ill-behave and black box optimization problems, which it is computationally more efficient than the genetic and annealing algorithms in *Matlab* **built-in** tool boxes. Moreover, *Matlab* built-in optimization function cannot evaluate vector costs, which means program would not be benefited from **SPMD**.

The method on transformation of optimization problems, and tunning of optimization method hyper-parameters (e.g. initial learning rate, σ; population size, λ) are all in-depth discussed in the coursework 1 report [4].

In order to benefit other users to implement **CMA-ES** optimization method, the objective oriented implementation is replaced with regular functional oriented implementation for this coursework. Also, features like pre-defined parameter boundaries and initial guess are also added in the fitting script.

4 Modelling Validation

With the model being developed, it is essential to test the model with practical results to test the accuracy of the model. Therefore, in this section, the simulated results are compared with the experimental results to verify the reliability of the module. The validation has been conducted on two different parts of the module, the viscoplastic model validation and the one-stage ageing model validation.

4.1 Viscoplastic Model Validation

Viscoplastic model predicts the yield strength developed in the material during the stamping process. The yield strength developed mainly depends on two variables, the stamping temperature and the strain rate. During the viscoplastic model validation, experimental stress and strain data was given at different strain rates, 0.01, 0.1 and 1. Material constants have been firstly auto-fitted according to the experimental data. The optimum material constants are shown in Table 2. These constants were then subsequently put back into the viscoplastic model for yield strength prediction. Figure 10 shows the comparison between the simulation results and the experimental results.

Table 2: Viscoplastic Model Material Constants

n1	n2	A	B	C	E	k	K
**	**	**	**	**	**	**	**

Because the measurement uncertainties was not given in the data set 1, the simulation error cannot be precisely concluded. But still, at strain rate 1 and 0.01, the module gives relatively accurate results. However, as strain increases, simulation error tends to increase at the same time. But in general, the simulation results agree with experimental ones.

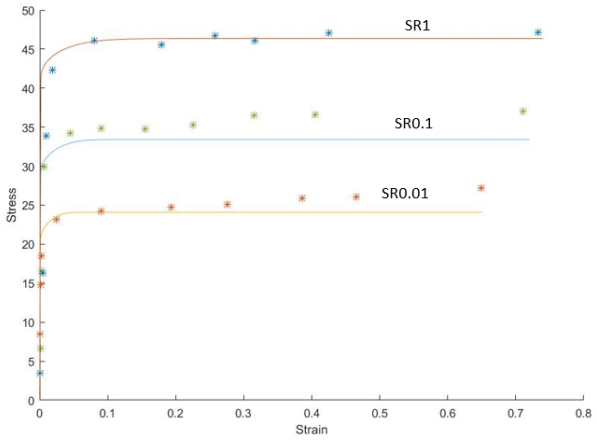

Figure 10: Comparison of simulation results with experimental results at strain rate 0.01, 0.1 and 1

4.2 One-Stage Ageing Model Validation

In the one-stage ageing model, simulation results are compared with the experimental data set at three temperatures, 180 °C, 220 °C and 240 °C. At each temperature, post-form strength was calculated in relation to the ageing time. Material constants used in this model are shown in Table 3. Results are plotted and compared on Figure 11, 12 and 13.

Table 3: Ageing Material Constants

A1	A2	A_d	B1	B2	C1	C2	C3	C4	C_s
**	**	**	**	**	**	**	**	**	**
C_i	C_{age}	f_{max}	K1	n2	Q_a	Q_s	T_s	σ_i	
**	**	**	**	**	**	**	**	**	

As shown in the graphs, the predicted results generally agree with the experimental data. As ageing time increases, post-form strength rises rapidly at the beginning and then starts to gradually decrease after reaching a peak value. In addition, as the ageing temperature increases from 180 °C to 240 °C, the peak post-form strength decreases. The largest peak post-form strength can be observed at 180 °C at approximately 122 HV.The predicted results highly align with the experimental data at 180 °C but this accuracy declines as ageing temperature increases with peak narrowing. It can also be observed that the ageing time required to reach the peak post-form strength decreases as temperature increases. Hence, increasing ageing temperature shortens peak ageing time but at the cost of peak post forming strength. Discussions about finding the optimum balance between these two parameters are in the following section.

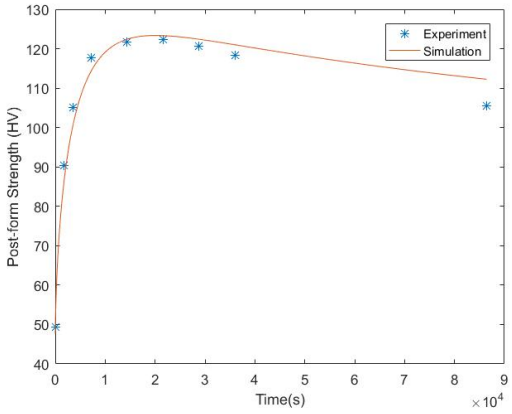

Figure 11: Comparison of simulation results with experimental results at 180 °C ageing temperature

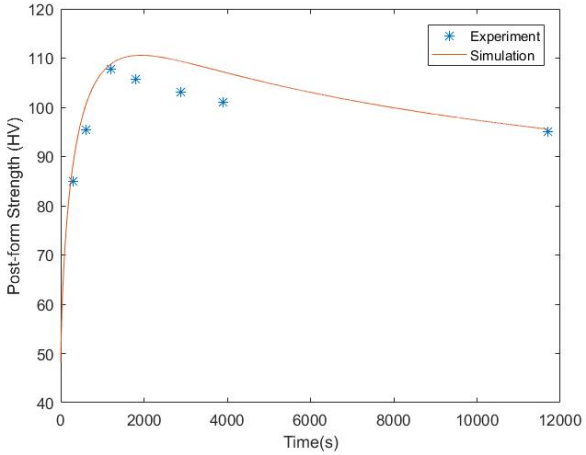

Figure 12: Comparison of simulation results with experimental results at 220 °C ageing temperature

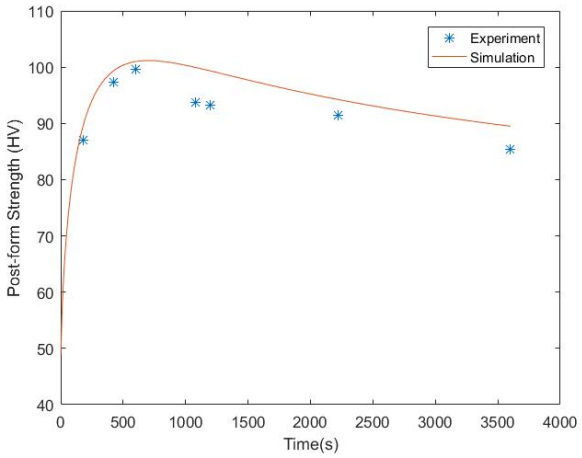

Figure 13: Comparison of simulation results with experimental results at 240 °C ageing temperature

5 Implementation of the functional modules

In this section, the post-form strength prediction model has been applied to the AA6082 model developed in coursework 2 [2]. As coursework 2 has found the optimum stamping-stage parameters that minimise the maximum thinning, this work uses the same stamping-stage parameters; for instance, the stamping velocity which determines the pre-straining in the stamping stage. Therefore the aim of this section is to find the optimum ageing process parameter set that gives the best post-form strength performance in the AA6082 part. The ageing-stage parameters include ageing time, ageing temperature and the number of ageing stages. These parameters were input into the model to investigate their effect on the post-form strength of the part.

5.1 Criteria

As the model uses the strain data from PAMSTAMP, the model predicts the yield strength on each finite element. Therefore, the post-form strength of different elements may be different. For instance, Figure 14 shows the results of a one-stage artificial-ageing (AA) with 400K ageing temperature and 1 hour ageing time. As shown from Figure 14, the post-form strength varies from 85 HV to 91 HV. Therefore, a criterion needs to be developed to quantify and represent the distribution of the post-form strength.

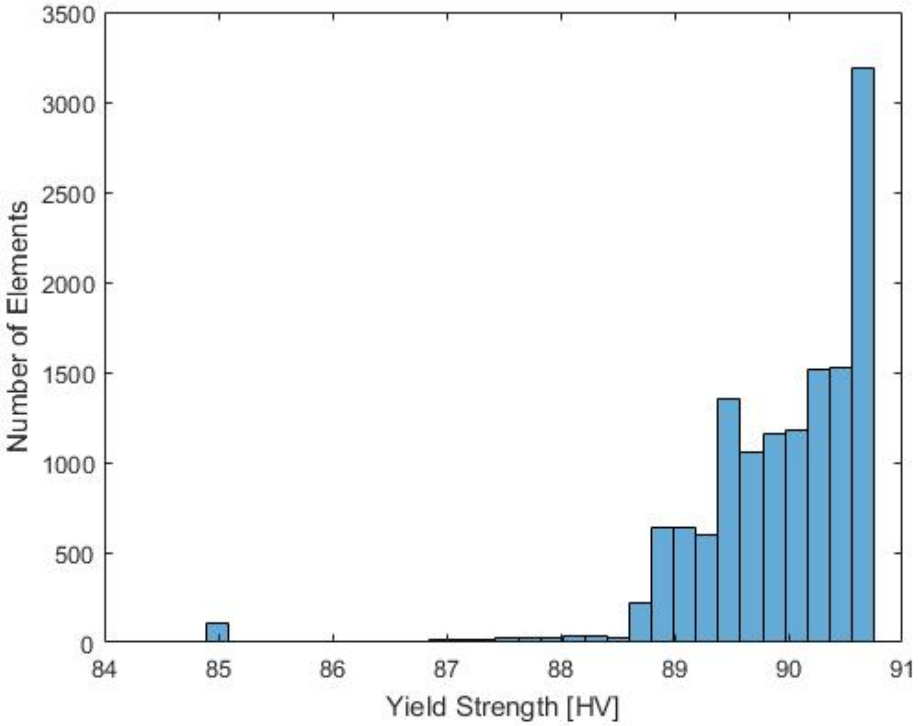

Figure 14: Post-form strength distribution across elements

These criteria should take both the minimum post-form strength and the overall average post-form strength into consideration. As in practical application, when loading reaches the lowest post-form strength, the material essentially fails. Therefore, the minimum post-form strength is an important indicator of the material post-form strength. In addition, when predicting the post-form strength, only the stamped region of the blank has been predicted and the stress at blank holding or the skirt region has been neglected. Therefore, the following equation has been used to quantify the post-form strength of the material.

$$Score = \sigma_{min} \times 0.7 + \sigma_{mean} \times 0.3 \tag{58}$$

where σ_{min} is the minimum post-form strength and σ_{mean} is the average post-form strength in stamped region. A 70% weight is assigned to σ_{min} and 30% weight to σ_{mean}. The score then represents the overall post-form strength of the material.

5.2 One-Stage Artificial Ageing

In one-stage ageing, two parameters, ageing temperature and ageing time, were input into the model in the range of 440K to 520K and 1s to 5 hours (18000s) respectively. The criteria score was calculated for each set of parameters and Figure 15 shows the results.

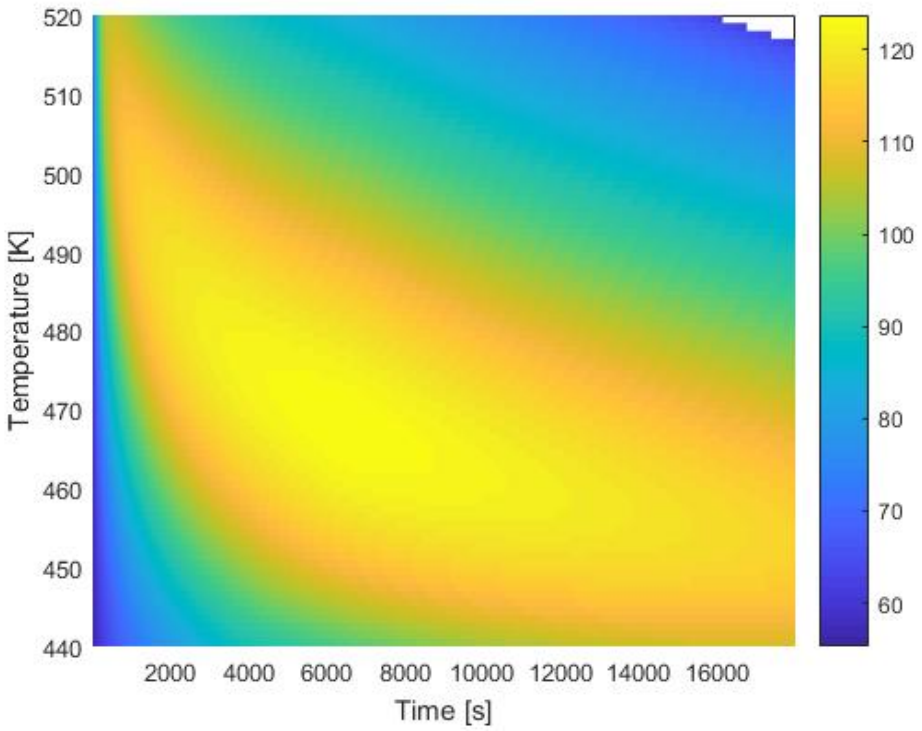

Figure 15: One-stage artificial ageing scores

As shown in figure 15, as ageing time increases, a lower ageing temperature is required to obtain peak post-form strength. This trend is most obvious at the low ageing time, in the range of 2000s to 5000s. The maximum score was obtained at 6580s (109 min) and 467K. The optimum parameters and results are shown in Table 4.

Table 4: Optimum parameters and results for one-stage AA

T (K)	t (s)	t (min)	Score (HV)
467	6580	109.67	123.77

5.3 Two-Stage Artificial Ageing

In the two-stage ageing process, there are four main parameters, the first-stage and the second-stage ageing temperature and time. It would be a five dimensional group, with four inputs and one output score. Even if the first-stage time or temperature is fixed, it would still be a four dimensional graph which is essentially the 3D version of Figure 15. Therefore, it is not practical to find the optimum two-stage ageing process parameters using the same method as outlined in one-stage ageing process. Therefore, in this section, a two-stage AA process similar to that in [2] has been simulated.

Instead of investigating the effect of each increments of the first-stage temperature and time, simulations have been tested at three temperature, 467K, 493K and 520K. Within each temperature, simulations have been tested at three ageing time, 60s, 180s and 300s. This is because the temperature in first-stage tends to be higher than that in the second-stage and the time tends to be shorter [2]. At 520K, simulations have also been run at 420s, 840s and 1800s to find the optimum parameter set. In the second stage, the simulation was run using the pre-set first-stage parameters to find the second-stage temperature and time that gives the highest post-form strength score. The associated parameters and results are shown in Table 5.

Table 5: Two-stage ageing process parameters and results

	Stage 1				Stage 2			
Set	T (K)	T (°C)	t (s)	t (min)	T (K)	t (s)	t (min)	Score (HV)
1	467	194	60	1	467	5520	92.00	122.07
2			180	3	467	5370	89.50	122.37
3			300	5	467	5220	87.00	122.66
4	493	220	60	1	474	4600	76.67	121.70
5			180	3	472	4610	76.83	122.32
6			300	5	471	4670	77.83	122.94
7	520	247	60	1	475	4540	75.67	120.82
8			180	3	472	4610	76.83	122.30
9			300	5	470	4710	78.50	123.42
10			420	7	468	4790	79.83	124.19
11			840	14	466	4930	82.17	125.25
12			1800	30	465	5000	83.33	125.47

As shown from Table 5, When the first-stage temperature is at 467K, it is found that the optimum temperature for stage 2 is always at 467K. This temperature is the same as the optimum temperature for one-stage AA. It is also found that as the ageing time in first-stage increases, the optimum ageing time in second-stage decreases and the overall ageing time decreases. In addition, the post-form strength score also increases. When the first-stage temperature is at 493K, the post-form strength follows a similar trend as before. As ageing time in first-stage increases, the score increases. However, the optimum ageing time also increases. Overall, there is a significant drop in optimum ageing time in the second stage. When the first-stage temperature is at 520K, which is also the theoretical maximum ageing temperature in the model, optimum ageing time in the second stage has a slight decrease. As before, the optimum ageing time also increases with the first-stage ageing time. At 420s first-stage ageing time, the peak post-form strength score exceeds that of the one-stage AA process. As the first-stage ageing time increases, the peak post-form strength score kept on increasing but at a much lower speed and at the cost of rapidly increasing overall ageing time.

Therefore, it can be concluded from Table 5, based on the observed trend, that the two-stage AA generally saves overall ageing time compared with one-stage AA at the cost of material post-form strength. Higher first-stage temperature with ageing time longer than 5min gives higher post-form strength. One of the limitation of this model is that it cannot accurately find the optimum parameters and score for the two-stage AA process as the simulation results do not converge. For instance, when the first-stage temperature is at 520K and time is at 10000s, the score still keeps on increasing at the value of 125.54 HV. Figure 16 shows the post-form strength score evolution with first-stage ageing time. It can be seen that the high score region shifts towards lower second-stage temperature as first-stage ageing time increases. But this region does not converge. However, in general, this simulation still serves as a good tool for

trend analysis and can be used to identify a range of optimum ageing temperature and time sets that gives the peak post-form strength.

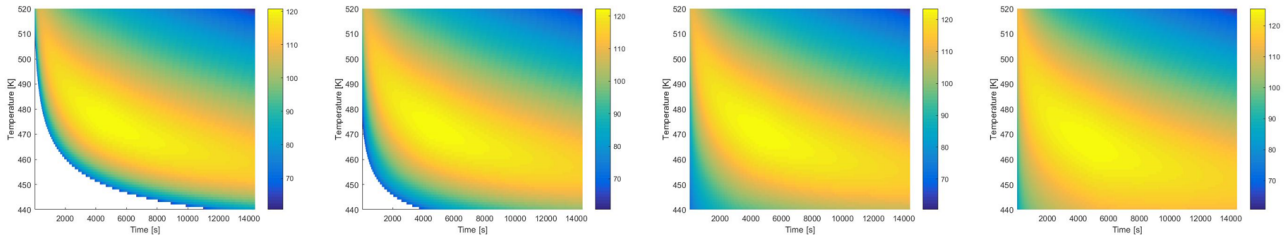

Figure 16: Two-stage AA score evolution with first-stage ageing time at 520K ageing temperature. From Left to Right, ageing time is at 60s, 180s, 300s, 1800s

5.4 Application of ageing module on PAMSTAMP

In previous sections, different parameter sets have been compared and discussed to find the optimum set that gives the highest post-form strength. This section applied the predicted post-form strength to the finite-element model, PAMSTAMP, to visualise the results. Parameter set 10 in table 5 is used in this section. The outcome is shown in figure 17. It can been seen from the graph that most of the low post-form strength is located on the blank skirt. This part was excluded from the score calculation in previous section. The stamp body has relatively consistent post-form strength in general.

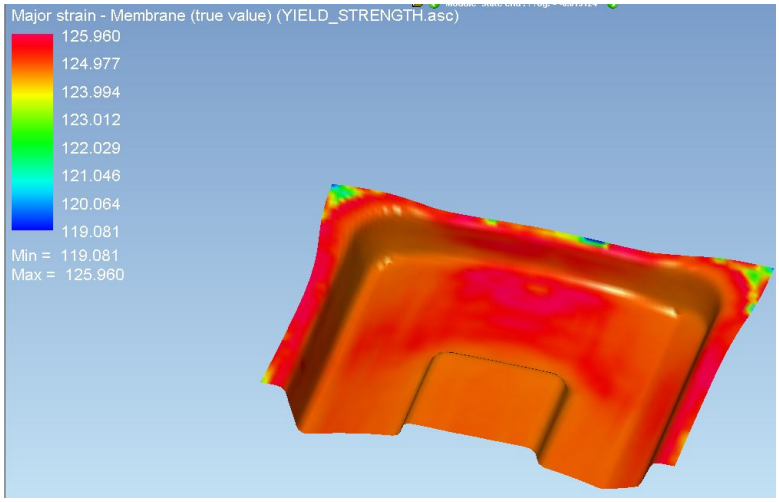

Figure 17: Predicted post-form strength plotted on PAMSTAMP

5.5 Implementation of Interfacial Heat Transfer Coefficient Model

The interfacial heat transfer (IHTC) model has been tested. The simulation process has been broken down into three stages. Firstly, input parameters required were the pressure range of the blank during the stamping process, the punching tool material and the oil thickness. An IHTC against pressure plot was calculated as the output; Figure 18 shows the plot. Secondly, this data set was imported to PAMSTAMP and ran a three-stage process, closing, stamping and quenching.Thirdly, temperature distribution of each element in each stage was then input to the MATLAB. Parameters such as the closing and stamping speed and the stroke distance

was also input in the model. The model then runs and checks the cooling rate of the quenching stage to see if they have met the criteria. If the criteria is met, then the output is 0, marked as 'Safe'. If not, the output is 1, marked as 'Failed'. Figure 19 shows the final results. Pink regions are the failure part and the blue regions are the safety part. All the failure regions are on the skirt which means the quenched part overall satisfies the criteria.

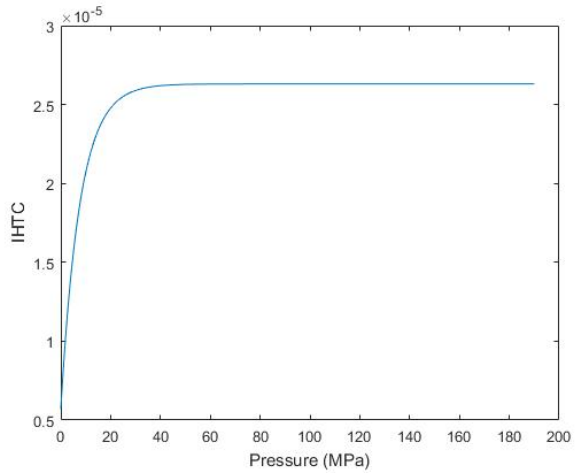

Figure 18: IHTC against Pressure

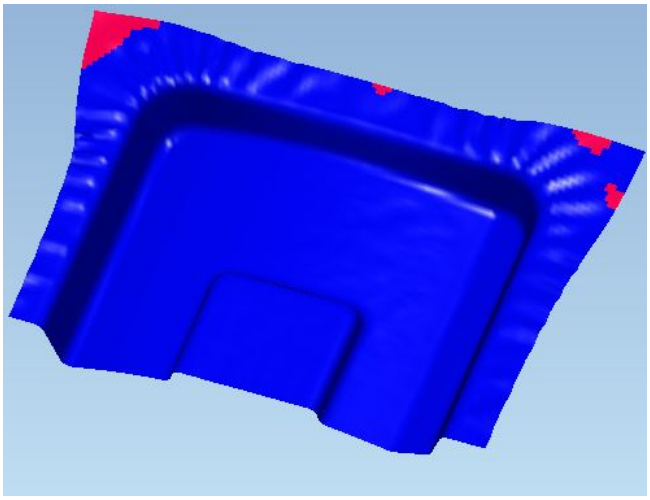

Figure 19: IHTC model output

6 Conclusion

In general, a viscoplastic model and an ageing model have been developed to predict the post-form strength of AA6082 aluminium alloys. The model was sufficiently accurate and simulation results mostly agree with the experimental data. Due to the vectorial design, the system running time has been significantly shortened and saved the analysis time.

The optimum operating conditions for both single-stage and two-stage artificial ageing process have been investigated. It is found that the two-stage process saves overall ageing time compared with the one-stage process usually at the cost of peak post-form strength. The optimum parameters for the one-stage process was found at 467K and 6580s. The optimum operating condition for the two-stage process was found at 520K and when the first-stage ageing time is above 420s. Future work needs to be done to improve the multi-stage process simulation accuracy and increase its capability to find the optimum operating conditions.

7 References

[1] Wu, L. & Ferguson, W. G. (2009) Modelling of Precipitation Hardening in Casting Aluminium Alloys. Materials Science Forum. 618-619 203-206. Available from: doi:10.4028/www.scientific.net/
619.203.

[2] Politis, D. & Zhang, Q. (2018) Introduction to the Modelling of Ageing. Imperial College London. pg 1-24.

[3] Myhr, O. R., Grong, Ø & Andersen, S. J. (2001) Modelling of the age hardening behaviour of Al–Mg–Si alloys. Acta Materialia. 49 (1), 65-75. Available from: https://www.sciencedirect.com/science/a
Available from: doi: 10.1016/S1359-6454(00)00301-3.

[4] Metal Processing Technology Coursework 1&2 - YUXUAN LIU, MOHAMED SAEED, XINYANG YUAN, HONGZE ZOU

[5] Kampmann, R.; Eckerlebe, H. & Wagner, R., (1987) Precipitation Kinetics in Metastable Solid Solutions-Theoretical Considerations and Application to Cu-Ti Alloys. In: Phase Transitions in Condensed Systems–Experiments and Theory: 525. Boston, Massachusetts; USA;

[6]Kampmann, R. & Wagner, R., (1984) Kinetics of Precipitation in Metastable Binary Alloys-Theory and Application to Cu-1.9at% Ti and Ni-14at% Al. 91.

[7] Shercliff, H. & Ashby, M. (1990) A process model for age hardening of aluminium alloys - II. Applications of the model. Acta Metall.Mater. 38 (10), 1803-1812.

[8] "Trapezoidal Rule." Wikipedia, Wikimedia Foundation, 16 Mar. 2018, en.wikipedia.org/wiki/Trapezoid

[9] "Gaussian Quadrature." Wikipedia, Wikimedia Foundation, 16 Mar. 2018, en.wikipedia.org/wiki/Gauss

[10] "Euler Method." Wikipedia, Wikimedia Foundation, 22 Mar. 2018, en.wikipedia.org/wiki/Euler_metho

[11] "The Runge-Kutta Method." Runge - Kutta, www.physics.drexel.edu/ steve/Courses/-Comp_Phys/Integrators/rk4.html.